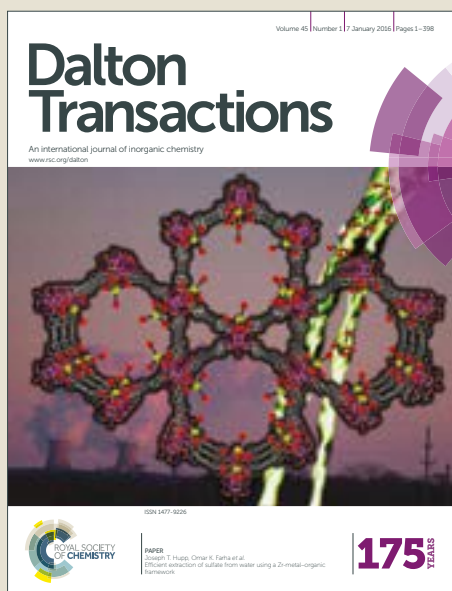


# Dalton Transactions

Accepted Manuscript



This article can be cited before page numbers have been issued, to do this please use: Y. Rachuri, S. Subhagan, B. Parmar, K. K. Bisht and E. Suresh, *Dalton Trans.*, 2017, DOI: 10.1039/C7DT03667A.



This is an Accepted Manuscript, which has been through the Royal Society of Chemistry peer review process and has been accepted for publication.

Accepted Manuscripts are published online shortly after acceptance, before technical editing, formatting and proof reading. Using this free service, authors can make their results available to the community, in citable form, before we publish the edited article. We will replace this Accepted Manuscript with the edited and formatted Advance Article as soon as it is available.

You can find more information about Accepted Manuscripts in the [author guidelines](#).

Please note that technical editing may introduce minor changes to the text and/or graphics, which may alter content. The journal's standard [Terms & Conditions](#) and the ethical guidelines, outlined in our [author and reviewer resource centre](#), still apply. In no event shall the Royal Society of Chemistry be held responsible for any errors or omissions in this Accepted Manuscript or any consequences arising from the use of any information it contains.



Journal Name

ARTICLE

## Selective and Reversible Adsorption of Cationic Dyes by Mixed Ligand Zn(II) Coordination Polymers Synthesized by Reactants Ratio Modulation

Received 00th January 20xx,  
Accepted 00th January 20xx

DOI: 10.1039/x0xx00000x

www.rsc.org/

Yadagiri Rachuri,<sup>a,b</sup> Sreevalsa Subhagan,<sup>b</sup> Bhavesh Parmar,<sup>a,b</sup> Kamal Kumar Bisht<sup>c</sup> and Eringathodi Suresh<sup>a,b\*</sup>

Dye capture and separation through coordination polymers (CPs) has been a promising research field in recent times due to the toxic and nondegradable nature of organic dyes released to the environment from various industries as well as the reusability of CPs for the said purpose. Here, we report the synthesis and characterization of two mixed ligand CPs  $\{[Zn_2(HBTC)_2(L)(H_2O)_2](C_2H_5OH)_3\}_n$  (**CP1**) and  $\{[Zn_5(BTC)_2(L)_3(OH)_4(H_2O)_2](H_2O)_4(CH_3OH)_{11}\}_n$  (**CP2**), (where, H<sub>3</sub>BTC = 1,3,5-benzene tricarboxylic acid and L = 1,4-bis(4-pyridyl)-2,3-diaza-1,3-butadiene) by stoichiometry variation of the precursors. Crystal structure revealed that **CP1** is a 2D network composed of  $[Zn_2(HBTC)_2(H_2O)_2]_n$  motif linked via terminal nitrogen atoms of L and **CP2** is a 3D framework in which symmetrically disposed two dimensional  $\{[Zn_5(BTC)_2(L)_3(OH)_4(H_2O)_2]\}_n$  sheets composed of pentanuclear  $[Zn_5(RCO_2)_6(\mu_3-OH)_2(\mu_2-OH)_2(H_2O)_2]$  SBUs are pillared by L ligands. Adsorption and separation of cationic dyes by **CP1** and solid-state fluorescence properties of both CPs have been investigated. Cationic dyes (RhB, MB, MV) can be effectively adsorbed by **CP1** from their aqueous solution (61%, 90%, and 97%) while anionic dye methyl orange (MO) remains uncaptured. Dye desorption studies and **CP1** as a column chromatographic filler for the separation of cationic dyes in water has also been demonstrated.

### Introduction

Environment protection has been a consensus of governments and scientists all over the world and billions of expenditures were cast to treat the pollution such as heavy metals,<sup>1–2</sup> organic waste water pollution<sup>3</sup>, nuclear radiation pollution<sup>4</sup> etc. Organic dyes are one of the major environmental pollutants in water because of their non-degradable nature and wide distribution. Synthetic organic dyes have been widely used in paper, printing, textiles, plastics and cosmetics industries. Due to large amount of dyes being used in textile and paper industries, dyed wastewater is discharged to natural water sources which are harmful not only to fish and other aquatic organisms but also for human health. Considering environmental and safety perspective, development of feasible technology is essential to remove dyes from liquid

waste before being discharged into nature. To perform this task, several approaches have been exploited such as chemical oxidation, photocatalytic degradation, biological treatment, adsorption etc.<sup>5–9</sup> Among these methods, adsorption perceived as one of the most feasible, effective, simple approach and number of materials such as activated carbon, zeolites, layered double hydroxides, porous organic polymers and metal-organic frameworks (MOFs) have been developed as dye adsorbents.<sup>10–16</sup> In view of anionic or cationic nature and different sizes of dye molecules, Coordination Polymers (CPs) or MOFs offering tunable pore size and framework charge are promising materials for adsorption and separation of dyes. Hence, based on the nature of CPs/MOFs as host, adsorption by different supramolecular interactions such as hydrogen bonding,  $\pi \cdots \pi$  stacking, electrostatic interactions etc. can be exploited in the selective uptake of dyes.<sup>16–18</sup>

CPs or MOFs are crystalline materials which are well known over the past decades due to their various applications in the area of gas storage/separation, removal of hazardous molecules, catalysis and biomedicine.<sup>19–34</sup> The tunability of pore size/shape by changing the connectivity of the inorganic moiety and sensible choice of the multidentate ligands in CPs/MOFs and thermal/chemical stability of these materials has captured particular interest towards diverse applications.<sup>35–37</sup> Highly structured and ordered CPs can be synthesized in many different mechanical or chemical procedures such as solvo-thermal method, slow evaporation

<sup>a</sup> Academy of Scientific and Innovative Research, CSIR-Central Salt and Marine Chemicals Research Institute, Council of Scientific and Industrial Research, G. B. Marg, Bhavnagar-364 002, Gujarat, India.

<sup>b</sup> Analytical and Environmental Science Division & Centralized Instrument Facility, CSIR-Central Salt and Marine Chemicals Research Institute, Council of Scientific and Industrial Research, G. B. Marg, Bhavnagar-364 002, Gujarat, India.

<sup>c</sup> Department of Chemistry, RCU Government Post Graduate College, Uttarakshi-249193, Uttarakhand, India.

Electronic Supplementary Information (ESI) available: [PXRD, FTIR, TGA, UV-Vis spectra, Calibration curves for standard dyes, Bond length, bond angle, H-bonding table, Zeta Potential values and Crystallographic information files]. See DOI: 10.1039/x0xx00000x

of a precursor solution, layering of solutions or slow diffusion of the components and mechano-chemical method.<sup>38–40</sup> Besides choice of the metal nodes with versatile coordination geometry and multidentate organic linkers, stoichiometry of the precursors, reaction condition such as temperature, solvents used in the reaction and pH of the reaction media etc. can play important role in fabrication and molding CPs/MOFs with multidimensional framework and topology. Structural alterations in CPs/MOFs have been studied and reported by manipulating reaction conditions such as temperature, solvent, pH and stoichiometry of the precursors in the synthetic approach.<sup>41–45</sup>

We have been involved in the fabrication of functional CPs/MOFs with different dimensionality utilizing N-donor ligands and multi-carboxylic acids. Recently, we have reported some mixed ligand luminescent coordination polymers for selective sensing and detection of noxious chemicals such as nitroaromatics, toxic heavy metals and chromium oxyanions.<sup>40,46–47</sup> In continuation of our ongoing research, herein we report Zn(II) based 2D and 3D CPs,  $\{[Zn_2(HBTC)_2(L)(H_2O)_2](C_2H_5OH)_3\}_n$  (**CP1**) and  $\{[Zn_5(BTC)_2(L)_3(OH)_4(H_2O)_2](H_2O)_4(CH_3OH)_{11}\}_n$  (**CP2**), (where, H<sub>3</sub>BTC = 1,3,5-benzene tricarboxylic acid and L = 1,4-bis(4-pyridyl)-2,3-diaza-1,3-butadiene) synthesized by mixed ligand strategy. Subtle changes in the molar concentrations of the reactants under the same experimental condition resulted in different products with diverse structures and networks. Accordingly, we were able to synthesize 2D and 3D Zn(II) CPs adopting the same layering technique by simply changing the stoichiometry of the precursors such as metal ion and ligands. The present study describes reactants ratio modulated synthesis of two CPs, their structural details, photoluminescence properties and the application of **CP1** for selective cationic dye adsorption in aqueous media.

## Experimental

### Material and General Methods

Precursors for synthesis of 1,4-bis(4-pyridyl)-2,3-diaza-1,3-butadiene (L) 4-pyridine carbaldehyde, hydrazine hydrate, as well as other chemicals such as 1,3,5-benzene tricarboxylic acid, metal salts and solvents were purchased from commercial sources. Distilled water was used for synthetic manipulations. The reagents and solvents were used as received without any further purification. L was synthesized by slight modification of the synthetic procedure described in literature and detail procedure is mentioned in supporting data.<sup>48</sup> CHN analyses were done using elemental vario MICRO CUBE analyzer. <sup>1</sup>H NMR spectra for the ligand L was recorded on Bruker AX500 spectrometer (500 MHz) at temperature 25 °C and was calibrated with respect to internal reference TMS. IR spectra were recorded using KBr pellet method on a Perkin Elmer, G-FTIR spectrometer. TG analysis was carried out using Mettler Toledo and Netzsch. X-ray powder diffraction (PXRD) data were collected using a PANalytical Empyrean (PIXcel 3D detector) system with CuK<sub>α</sub> radiation. Single crystal structures

were determined using BRUKER SMART APEX (CCD) diffractometer. Liquid and solid-state UV-Vis spectra were recorded using Varian model CARY 500/ Shimadzu UV-3101PC spectrometer and photoluminescence spectra were recorded at room temperature utilizing Fluorolog Horiba Jobin Yvon spectrophotometer. Field Emission-Scanning Electron Microscopy (FE-SEM) was used for SEM images of **CP1** morphology studies. Zeta potential (ζ) measured using a Zetasizer Nano ZS light scattering apparatus (Malvern Instruments, U.K.) with a He-Ne laser (633 nm, 4 mW) at 298.15 K.

### Synthesis of CP1 and CP2

#### Preparation of Stock ligand solution for CP1 (SL1):

H<sub>3</sub>BTC (42 mg, 0.2 mmol) was added to NaOH (25 mg, 0.64 mmol) in 20 mL of water with constant stirring to make clear solution. L (42 mg, 0.2 mmol) was dissolved in 20 mL ethanol separately. Both solutions were mixed together by constant stirring for 15 minutes, filtered and used as stock ligand solution.

#### Preparation of Stock ligand solution for CP2 (SL2):

H<sub>3</sub>BTC (210 mg, 1 mmol) was added to NaOH (144 mg, 3.6 mmol) in 20 mL of water with constant stirring to make clear solution. L (210 mg, 1 mmol) was dissolved in 20 mL ethanol separately. Both solutions were mixed together by constant stirring for 15 minutes, filtered and used as stock ligand solution.

#### Growth of CP1 Single Crystals:

2 mL of stock ligand solution (SL1) was carefully layered above the 4 mL of Zn(NO<sub>3</sub>)<sub>2</sub>·6H<sub>2</sub>O (120 mg in 10 mL, 0.4 mmol) solution with 4 mL buffer (methanol & water 1:1) between the layers in a narrow test tube. The test tube was covered and kept for slow diffusion of reactants at room temperature which afforded yellowish block shaped crystals within a week time (Yield ~76%). Elemental analysis (%) Cal. for C<sub>36</sub>H<sub>40</sub>N<sub>4</sub>O<sub>17</sub>Zn<sub>2</sub>: C, 46.42; H, 4.33; N, 6.01; found: C, 43.8; H, 4.70; N, 5.67; IR cm<sup>-1</sup> (KBr): 3451(b), 1631(s), 1579(s), 1449(s), 1381(s), 1111 (w), 1023 (w), 759(s), 719(s), 573(m) and 482(m).

#### Growth of CP2 single Crystals:

2 mL of stock ligand solution (SL2) was carefully layered above 4 mL of Zn(NO<sub>3</sub>)<sub>2</sub>·6H<sub>2</sub>O (297 mg in 10 mL, 1 mmol) solution with 4 mL buffer (methanol & water 1:1) in between. Pale Yellowish block shaped crystals were harvested by diffusion of reactants in the test tube within two weeks (Yield ~45%). Elemental analysis (%) Cal. For C<sub>65</sub>H<sub>96</sub>N<sub>12</sub>O<sub>33</sub>Zn<sub>5</sub>: C, 41.08; H, 5.09; N, 8.84; found: C, 41.43; H, 4.28; N, 8.92; IR cm<sup>-1</sup> (KBr): 3382(b), 1622(s), 1573(s), 1444(s), 1376(s), 1108(w), 1023(w), 764(m), 721(m), 570 (w), 518 (w) and 474 (w).

#### Bulk Synthesis of CP1 by conventional (reflux) method:

For synthesis of **CP1** in bulk quantity, 105 mg of (0.5 mmol) H<sub>3</sub>BTC was initially mixed with 15 mL aqueous solution of 84 mg (1 mmol) of NaHCO<sub>3</sub>. To this 15 mL of methanolic solution of 105 mg (0.5 mmol) of L was added slowly, followed by 297 mg (1 mmol) of 15 mL aqueous solution of zinc nitrate resulting a pale yellowish turbid precipitate immediately. The mixture was allowed to reflux with stirring for 6 h at 70 °C. The

mixture was centrifuged, washed with water followed by methanol for several times and dried under ambient conditions (Yield ~89%). Elemental analysis (%) Cal.: C, 46.42; H, 4.33; N, 6.01; found: C, 44.83; H, 3.53; N, 6.53; IR  $\text{cm}^{-1}$  (KBr): 3448 (b), 1630 (s), 1565 (s), 1439 (s), 1380 (s), 1100 (w), 1023 (w), 758 (s), 725 (s), 577 (m), 492 (m).

### Dye adsorption experiments

Freshly prepared compound **CP1** (100 mg) was transferred to the aqueous solutions of methyl orange (MO), methylene blue (MB), rhodamine B (RhB) and methyl violet (MV) (10 mL,  $5 \times 10^{-5}$  M), respectively. The dye solutions containing the adsorbents were mixed well by constant stirring for 3 hours. After adsorption for a pre-determined time, solutions were allowed to centrifuge to isolate the solid CPs from the liquid and the concentration of the dye was determined by UV-Vis spectroscopy. After completion of adsorption process the amount of the dye adsorbed onto the **CP1** was determined according to the change of concentration before and after adsorption experiment. The amount of dye adsorbed after 3 h,  $q_e$  (mg/g), was obtained by the following equation.

$$q_e = (C_i - C_e)V \times MW/m \quad (1)$$

where  $C_i$  and  $C_e$  are initial and equilibrium concentrations of dyes (moles/L).  $V$  is the volume of the solution (L),  $MW$  is the molecular weight of dyes and  $m$  is the mass of adsorbent used (g).

The removal percentage  $\eta$  of dyes was calculated using the following equation:

$$\eta = (C_i - C_e)/C_i \times 100\% \quad (2)$$

### Dye release study

The dye adsorbed samples, **CP1@MV**, **CP1@MB** and **CP1@RhB** (10 mg) were transferred into 0.5 mL MeOH in a cuvette separately. UV-Vis spectra were employed to monitor the desorption ability of **CP1@ dye** at scheduled time intervals.

### Chromatographic column for dye separation

A chromatographic column (15 cm height and 0.5 cm diameter) was packed with aqueous slurry of **CP1** (up to 5 cm), for the individual separation experiments. In each independent experiment aqueous solutions of the respective dyes RhB, MB, MV and MO ( $10^{-4}$  M) was passed through the column at the room temperature. To study the separation experiments of mixture of dyes, MO+RhB, MO+MB and MO+MV (1:1 v/v) were allowed to pass through the chromatographic column. The time taken for the whole separation is approximately 15 min. The UV-Vis spectra of effluents were studied to confirm the separation capability.

### X-ray crystallography

Summary of crystallographic data and selected bond lengths and bond angles for **CP1** and **CP2** are given in Table S3 and S4. Single-crystal X-ray data collection was performed on a Bruker SMART APEX CCD diffractometer equipped with graphite

monochromatized MoK $\alpha$  radiation ( $\lambda = 0.71073 \text{ \AA}$ ) at 150 K for both the CPs. No crystal decay was observed during the data collections. The SMART and SAINT software packages were used for data collection and reduction, respectively<sup>49</sup>. In both cases, absorption corrections based on multi scans using the SADABS software was also applied.<sup>50</sup> The structures were solved by direct methods SHELXL-2017/1 and were refined on  $F^2$  by the full-matrix least-squares technique.<sup>51</sup> All non-hydrogen atoms were refined anisotropically till convergence is reached. The hydrogen atoms of the organic moiety for both CPs were either located from difference Fourier map or fixed stereo chemically. Hydrogen atoms for the coordinated water molecules were located from the difference Fourier map and the O-H distances were kept fixed using DFIX command. In the case of **CP1**, the lattice solvent molecules were highly disordered and the diffused peaks appeared was modelled sensibly by assigning them as ethanol moiety which is used in the preparation of stock solution in crystallization experiment. Hydrogen atoms of coordinated hydroxyl group is located and included in the structure of **CP2**. After the complete refinement of **CP2** along with the located lattice solvent molecule, large number of diffused peaks with residual electron density ranging from  $\sim 3.5 \text{ e/\AA}^3$  to  $2 \text{ e/\AA}^3$  were observed in the difference Fourier map which can be attributed to disordered solvent molecule present in the crystal lattice. Attempts to model these disordered peaks were unsuccessful since residual electron density was weak and there were no obvious major site occupations for the lattice solvent molecule. PLATON/SQUEEZE<sup>52</sup> was used to mask the diffraction data for the contribution from disordered lattice solvent (methanol) molecule. The solvent accessible void volume and the corresponding electron counts/unit cell estimated was  $426 \text{ \AA}^3/141\text{e}$  for **CP2**. This electron count corresponds to approximately eight disordered methanol molecules present in the unit cell as solvent of crystallization for **CP2**. Final cycles of least-square refinements with the modified data set after masking the contribution from the disordered solvent molecules significantly improved the R-values and Goodness of Fit of the structural data in **CP2**. The molecular formula provided in the crystallographic table includes the lattice solvent molecules.

## Results and discussion

### Crystal and Molecular Structure of $\{[\text{Zn}_2(\text{HBTC})_2(\text{L})(\text{H}_2\text{O})_2(\text{C}_2\text{H}_5\text{OH})_3]_n\}$ (**CP1**)

The X-ray structure of **CP1** reveals a 2D framework in which the asymmetric unit is composed of one crystallographically unique Zn(II), one monoprotonated trimesic acid (HBTC), half a molecule of N-donor ligand L (with a twofold axis bisecting the azine bond), one coordinated water and 1.5 lattice ethanol molecule. Each Zn1 within the basic dimeric unit, holds a distorted trigonal bipyramidal coordination are linked through pairs of symmetrically disposed HBTC ligands with opposite orientations via  $\mu_3\text{-}\eta^2\eta^0\eta^1\eta^0$  mode of coordination through carboxylate oxygen O5 and O1 in the formation of 1D stepped substructure running along b-axis (Fig. 1a&1b).

$[\text{Zn}_2(\text{HBTC})_2(\text{H}_2\text{O})_2]_n$  motif is further axially coordinated to N atoms from L to complete the distorted  $[\text{ZnNO}_4]$  trigonal bipyramidal geometry around the metal center generating a 2D supramolecular architecture. Notably, the L coordinate in bidentate mode along *c*-axis with  $[\text{Zn}_2(\text{HBTC})_2(\text{H}_2\text{O})_2]_n$  motif alternately in an outward fashion along two sides through the terminal nitrogen atoms generating the 2D corrugated rectangular network in **CP1** (Fig. 1c). The coordination sphere of each central Zn(II) atom is provided by four oxygen atoms (O5, O5#, and O1 from HBTC and O7 from water) and one nitrogen N1 from L, displaying a distorted trigonal bipyramidal geometry. The deviation of Zn(II) from the mean coordination trigonal plane, O5–O1–N1, is 0.250 Å, and the axial  $\angle\text{O5\#–Zn1–O7}$  angle 175.18(6)°. Nearest Zn···Zn separation within the dimeric unit is 3.493(4) Å and within the double layered  $[\text{Zn}_2(\text{HBTC})_2]_n$  motif bridged by HBTC is 9.643(5) Å.

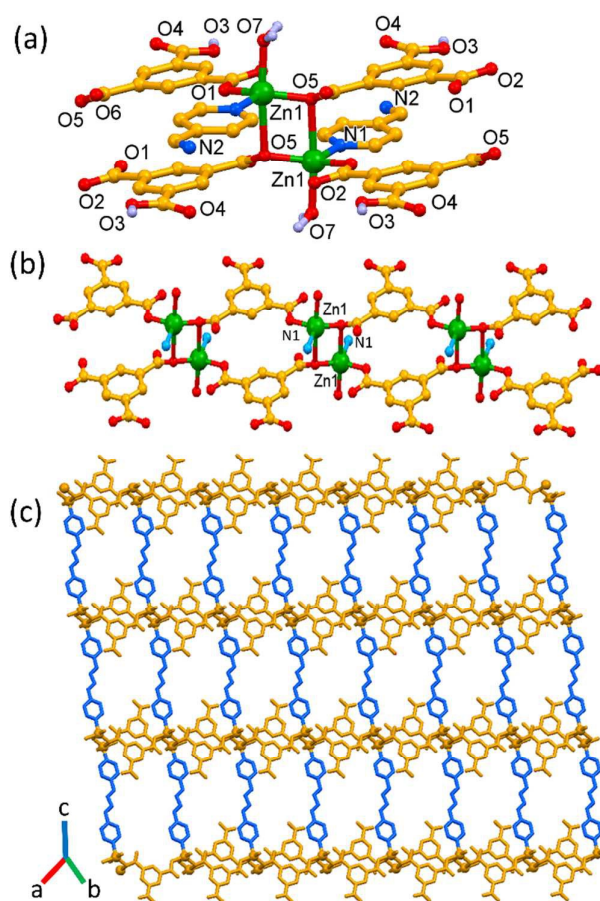


**Fig. 1** (a) Coordination environment around metal center depicting trigonal bipyramidal geometry in **CP1**, (b) A layered  $[\text{Zn}_2(\text{HBTC})_2(\text{H}_2\text{O})_2]_n$  1D stepped substructure running along *b*-axis and (c) Two-dimensional pillar-layer type corrugated rectangular network in **CP1**.

Exobidentate nitrogen atoms of L crosslinked between the adjacent  $[\text{Zn}_2(\text{HBTC})_2(\text{H}_2\text{O})_2]_n$  motif with Zn···Zn distance 15.439 Å generating the two dimensional motif in **CP1**. The through-space apertures within the 2D nets measure 15.439 Å × 9.643 Å and the lattice methanol molecule. In an attempt to understand the supramolecular interaction packing and hydrogen bonding interactions are analyzed. Interestingly,

strong intermolecular dimeric association involving O–H···O interaction is observed between partially occupied hydrogen of the carboxylic acid from the uncoordinated HBTC moiety between the neighboring two dimensional networks. Further, coordinated water hydrogen act as a donor and involved in intermolecular O–H···O contacts and the disordered lattice ethanol molecule which is anchored within the rectangular cavity of the 2D nets. In addition to this O–H···O contact phenyl hydrogen H14 of L is making a C–H···O interaction across the dimeric unit with the carboxylate oxygen O6 to stabilize the 2D framework in the crystal lattice.

### Crystal and Molecular Structure of $\{[\text{Zn}_5(\text{BTC})_2(\text{L})_3(\text{OH})_4(\text{H}_2\text{O})_2] (\text{H}_2\text{O})_4(\text{CH}_3\text{OH})_{11}\}_n$ (**CP2**)

**CP2** represents a 3D coordination framework and crystallizes in the triclinic space group  $P\bar{1}$ . The asymmetric unit of **CP2** consists two Zn cations (Zn1 and Zn2 at general position) and half of Zn3 at special position (0.5, 0.5, 1.0), one completely deprotonated BTC, one and a half molecules of L, two bridging hydroxyl ions, one coordinated water molecules along with two water molecules and two methanol molecules as solvent of crystallization. The framework  $\{[\text{Zn}_5(\text{BTC})_2(\text{L})_3(\text{OH})_4(\text{H}_2\text{O})_2] (\text{H}_2\text{O})_4(\text{CH}_3\text{OH})_{11}\}_n$  is based on a secondary building unit (SBU),  $[\text{Zn}_5(\text{RCO}_2)_6(\mu_3\text{-OH})_2(\mu_2\text{-OH})_2(\text{H}_2\text{O})_2]$  composed of a pentanuclear Zn(II) cluster, in which Zn3 is occupying the center of symmetry and surrounded by four symmetrically disposed Zn nodes (Zn1 and Zn2) bridged *via* carboxylate as well as hydroxyl oxygen atoms. The pentanuclear Zn(II) cluster with coordination geometry around the metal center is depicted in Fig. 2a. The central metal ions Zn3 and Zn2 are hexacoordinated and adopt a distorted octahedral geometry while the coordination around Zn1 is distorted trigonal bipyramidal. Thus, in Zn3, the square base is composed of the symmetrically oriented carboxylate and hydroxyl oxygen atoms O3 and O8 (Zn3–O3 = 2.075(5), Zn3–O8 = 2.062(5)) which also acts as a bridging ligand with the neighboring Zn1 in the cluster formation. Another symmetric hydroxyl oxygen O9 at the axial position (Zn3–O9 = 2.138(5)) completes the octahedral geometry around Zn3 metal center. Hence, carboxylate oxygen O3 and hydroxyl oxygen O9 is involved in  $\mu_2$ -type bridging connecting Zn1, Zn3 and Zn2, Zn3 respectively while hydroxyl oxygen O8 is making  $\mu_3$ -coordination linking all the three metal centers Zn1, Zn2 and Zn3. Octahedral coordination of Zn2 is provided by carboxylate oxygen atoms O2 and O4 of different BTC ligands, hydroxyl oxygen atoms O8 and O9, O7 from water and monodentate coordination through N3 from the dangling L. Square base around Zn2 is constituted by O2, O4, O7 and O8 and the axial coordination provided by N3 from L and hydroxyl oxygen O9. Zn1 possesses a trigonal bipyramidal coordination in which the trigonal base is provided by carboxylate oxygen atoms O1, O6 and hydroxyl oxygen O8 with the metal ion up by 0.287 Å from the trigonal base towards the axially coordinated N1 with axial angle  $\angle\text{N1–Zn1–O3} = 171.54^\circ(5)$ . The nearest Zn(II)···Zn(II) distance of the symmetrically oriented pentanuclear cluster is Zn1···Zn2 = 3.441 Å, Zn1···Zn3 = 3.324 Å and Zn2···Zn3 = 3.113 Å respectively. As represented, the pentanuclear SBUs (Fig. 2a)

are extended into a 2D sheet by versatile bridging mode of the carboxylate oxygen atoms from the completely deprotonated BTC moiety and the hydroxyl oxygen atoms O8 and O9.

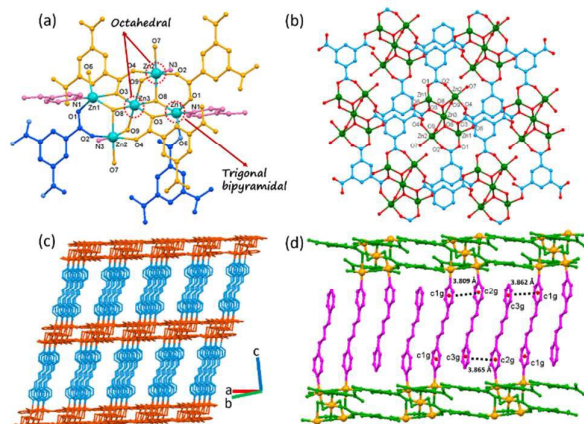


**Fig. 2** (a) Coordination geometry around the Zn(II) metal center in the formation of symmetrically disposed pentanuclear metal cluster in **CP2**, (b) 2D sheet like architecture generated in **CP2** by the coordination of completely deprotonated BTC ligand and hydroxyl groups, (c) 3D coordination polymeric net observed in **CP2** and (d)  $\pi\cdots\pi$  stacking interaction between the pyridyl rings between different L ligand moieties of **CP2**.

Accordingly, from the BTC ligand carboxylate oxygen O1, O2 is involved in  $\mu_2\text{-}\eta^1\eta^1$ , O3, O4 in  $\mu_3\text{-}\eta^2\eta^1$  and O5, O6 is making  $\eta^1\eta^0$  mode of binding and hydroxyl oxygen atoms O8 and O9 are involved in  $\mu_3$  and  $\mu_2$  mode of coordination in extending the pentanuclear metal clusters in the formation of 2D sheet like network in **CP2** (Fig. 2b). Two dimensional sheets thus formed is further pillared alternatively from through N1 of the symmetrical L ligand in bidentate mode with Zn1 with the neighboring sheets generating a 3D coordination polymeric net (Fig. 2c). Interestingly, pairs of the dangling L ligands with opposite orientation occupied between the square grid through unidentate coordination with Zn2 and involved in  $\pi\cdots\pi$  stacking interaction between the pyridyl rings from either side (Fig. 2d) (Cg...Cg distance ranging from 3.80 to 3.86 Å). The coordinated and the lattice water molecules O7 and O11 act as donors and involved in strong O-H...O interactions. Thus, H7B from O7 is making O-H...O contact with the O1AA of the methanol and both hydrogen atoms H11A and H11B is making O-H...O interaction with methanol oxygen O0AA and the hydroxyl oxygen O9 respectively. Interestingly lattice water hydrogen H10A is making O-H...N contact with N6 of the dangling L. All these hydrogen bonding interactions stabilizes the molecule in the crystal lattice and details of pertinent hydrogen bonding interactions are given in Table S1.

#### PXRD, IR and TGA analyses

**CP1** synthesized by flexible methods and **CP2** have been characterized by various analytical methods including X-ray crystallography. Phase purity of **CP1** synthesized by different methods and **CP2** crystals obtained by diffusion has been confirmed by comparing the experimental PXRD profile with simulated patterns of single crystal X-ray diffraction (SXRD)

(Fig. S1a&b). The chemical composition of **CP1** and **CP2** were also estimated and ascertained by TGA, elemental and single crystal analyses. FTIR spectra for **CP1** and **CP2** were recorded by suspending the compounds in KBr pellets (Fig. S2). For **CP1** and **CP2** two pairs of  $\nu_{\text{asym}}$  and  $\nu_{\text{sym}}$  frequencies appeared at 1631, 1449  $\text{cm}^{-1}$  ( $\Delta\nu = 182$ ), 1579, 1381  $\text{cm}^{-1}$  ( $\Delta\nu = 198$ ) and 1622, 1444  $\text{cm}^{-1}$  ( $\Delta\nu = 178$ ), 1573, 1376  $\text{cm}^{-1}$  ( $\Delta\nu = 197$ ) respectively, corresponding to the carbonyl functionality of the BTC ligand. Broad bands observed for both CPs in the region, 3693–3307  $\text{cm}^{-1}$  are attributable to the O–H stretching modes of coordinated or lattice water molecules. The weak absorption bands in the fingerprint region, at 573, 482  $\text{cm}^{-1}$  for **CP1**, 570, 518, 474  $\text{cm}^{-1}$  for **CP2** are assigned to Zn–O and Zn–N vibration modes. Thermogravimetric analyses (TGA) were performed in the range of 30–700 °C in inert atmosphere in order to gauge the thermal behavior and stability of CPs (Fig. S3). The TG curve of **CP1**, exhibits weight loss in the range of 50–130 °C which is corroborated to the lattice methanol and coordinated water molecules (cal. 17.4%, obs. 15.02%), subsequently the framework decomposed at ca. 330 °C. **CP2** expelled lattice methanol and coordinated/uncoordinated water molecules in the range of 45–251 °C (cal. 18.02%, obs. 18%), followed by the decomposition of the 3D network at ca. 340 °C.

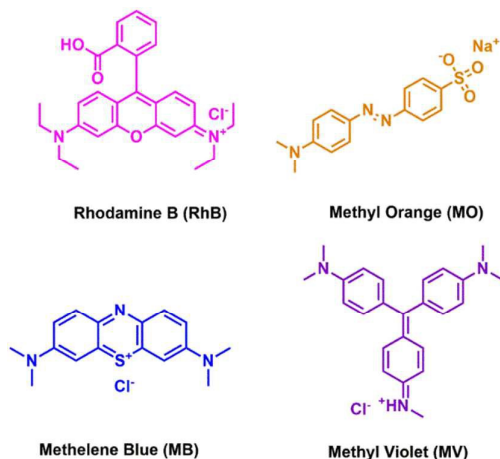
#### Photoluminescence properties

Photoluminescence properties of MOFs comprising of  $d^{10}$  metal ions and electron rich multidentate ligands have been extensively studied due to strong emission properties and potential applications in the field of photo luminescent chemical sensors.<sup>53–57</sup> Luminescence properties of **CP1**, **CP2**, L and H<sub>3</sub>BTC were investigated in the solid state and in the suspension of DMF at room temperature. The emission peaks for free ligands L and H<sub>3</sub>BTC in the solid state appeared at 410, 388 nm upon excitation 300, 320 nm respectively, which can be assigned to the ligand centered  $\pi^*\rightarrow\pi$  or  $\pi^*\rightarrow n$  electronic transitions. **CP1** and **CP2** exhibited emission band nearly at the same wavelength ca. 445 nm upon excitation at 320 nm (Fig. S4 & Fig. S5). Nevertheless, suspension of both CPs in DMF (~414 nm) showed shift in emission maximum (~31nm) which can be due to solvent effect. In comparison with the emission of free ligands L and H<sub>3</sub>BTC, the change in emission wavelengths for **CP1** and **CP2** can be attributed to the ligand to metal charge transfer phenomenon (LMCT).<sup>58–59</sup>

#### Selective dye adsorption from aqueous solutions by **CP1**

Removal of organic dyes from industrial effluents is ongoing research in the area of separation technology. Recently, MOFs/CPs have been employed for the separation of hazardous chemical species from air and industrial effluents. Especially, charged or functional CPs have been reported as potential materials for selective adsorption of cationic or anionic dyes from aqueous solutions.<sup>60–62</sup> Generally, there are three main aspects for the adsorption process: size selectivity, ion exchange and the electrostatic attraction. Dye adsorption from aqueous solutions has been reported in the literature, based on the adsorption process.<sup>63–65</sup> These investigations

revealed that dyes show selective adsorption depending on the nature of framework. For instance, anionic frameworks prefer cationic dyes and *vice-versa*.<sup>66-67</sup> Neutral functionalized frameworks towards selective adsorption of cationic dyes over anionic dyes is reported scarcely.<sup>68-69</sup>



**Scheme 1** Molecular structures of dyes used in the present investigation.

In the present investigation, we have explored **CP1** as a selective adsorbent for cationic dyes from aqueous solutions. An efficient adsorbent material should enjoy outstanding adsorption property toward the dyes, good chemical stability and competence for selective removal and separation. To perform adsorption and separation experiments four organic dyes have been selected, *viz.*, cationic dyes RhB, MB, MV and anionic dye, methyl orange (MO) (Scheme 1).

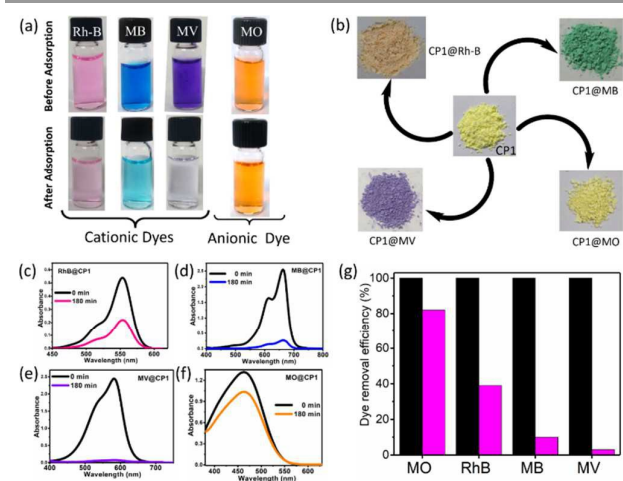


**Fig. 3** (a) The digital photographs of dye solutions before and after adsorption representing the cationic dye adsorption over anionic dye by **CP1**, (b) Color change observed in **CP1@Dye** material after respective dyes adsorption by **CP1**, (c-f) UV-Vis spectral changes based on treating **CP1** with different cationic/anionic dyes after 3h and (g) Removal efficiency plot of MO, RhB, MB and MV after 3h by **CP1** (black bars: initial concentration; Pink bars: concentration after 3 h).

To evaluate the adsorption capacity, 100 mg of **CP1** was suspended into 10 mL of aqueous solutions of the respective

dye ( $5 \times 10^{-5}$  M) and allowed to mix by constant stirring at room temperature for 3 h in dark condition. After the mentioned scheduled time for dye adsorption process, color intensity for two cationic dyes (RhB, MB) was reduced to some extent and appreciable color change was observed in the case of MV (which almost became colorless). Contrastingly, no color change was shown in the case of the anionic dye MO (Fig. 3a). Above results clearly indicate the potential of neutral **CP1** as an adsorbent towards cationic dyes over the anionic one. The concentration of dyes after adsorption experiment was assessed by UV-Vis spectrometry. The drop-in dye concentration observed (from  $5 \times 10^{-5}$  M initial concentration) within 3 h time is  $1.97 \times 10^{-5}$  M,  $4.67 \times 10^{-6}$  M,  $1.55 \times 10^{-6}$  M and  $\sim 4.78 \times 10^{-5}$  M for the respective dyes RhB, MB, MV and MO (Fig. 3c-f). Calibration experiments were performed to assess the amount of adsorbed dye after a given time using the absorbance of standard aqueous solutions of dyes (Fig. S6). Based on the equation (2) the calculated adsorption efficiency ( $\eta$ ) for RhB, MB and MV were 61%, 90%, and 97% respectively, whereas for MO was  $\sim 20\%$  (Fig. 3g). The adsorption amount of cationic dyes ( $q_e$ , mg/g) by **CP1** was calculated based on equation (1) and was found to be 1.45, 1.5 and 2 mg/g for RhB, MB and MV respectively. At higher dye concentrations ( $10^{-4}$  M) the efficiency of adsorption was increased which turns out to be 2.8, 2.65 and 3.52 mg/g respectively. These experiments clearly demonstrated the potential of neutral network **CP1** for the effective removal application of cationic dyes. As depicted in Fig. 3b, the color of the dye adsorbed **CP1** (**CP1@dye**) in presence of the respective cationic dyes changed completely from pale yellow, whereas no substantial color change was observed in the case **CP1@MO**.

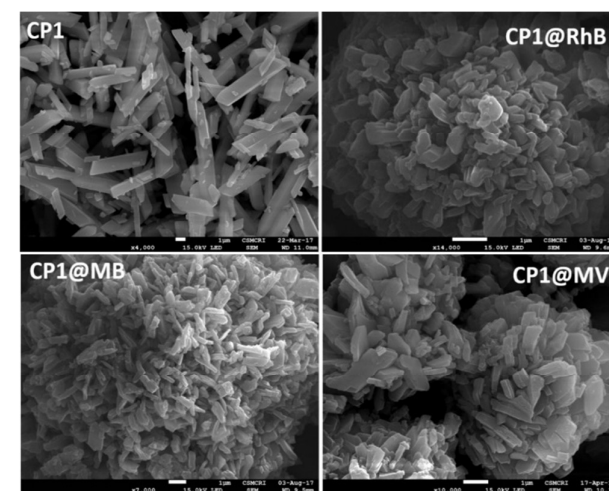


**Fig. 4** FE-SEM micrographs of **CP1**, before and after adsorption of cationic dyes.

As a result of dye adsorption, pale yellow **CP1** is converted to light brown, green and violet colored material in the case of **CP1@RhB**, **CP1@MB** and **CP1@MV**. Furthermore, the **CP1@dye** materials were characterized by solid state UV-Vis, FTIR spectra and TG analysis (Fig. S7, S8&S9) and the morphology of **CP1** before and after adsorption of cationic dyes have been studied by FE-SEM analysis (Fig. 4). FE-SEM

micrographs of **CP1@dy**e indicated the agglomeration with spherical morphology of micro-crystalline **CP1**. PXRD patterns of **CP1@dy**e showed the preservation of framework structures implying that **CP1** retains the structural integrity and can be used efficiently for the removal of MV from the group of dyes selected in present investigation (Fig. S10). Study of dye adsorption and separation using functionalized CPs with good selectivity toward the targeted dyes become a promising research topic. The selective adsorption of organic dye from the mixture becomes important considering the recovery of valuable chemicals from industrial waste water. The selectivity of **CP1** towards cationic dyes encouraged us to investigate separation study of cationic and anionic dye mixture. For the selective adsorption, anionic dye methyl orange was taken along with other three cationic dyes in equimolar ratio (1:1:1, 10 mL) for the separate batch studies. **CP1** (100 mg) was added in mixture of aqueous dye solutions and allowed to mix thoroughly by stirring for 3 h in dark condition. Selective adsorption of the cationic dyes from organic dye mixture by **CP1** was also monitored by UV-Vis spectrophotometer.

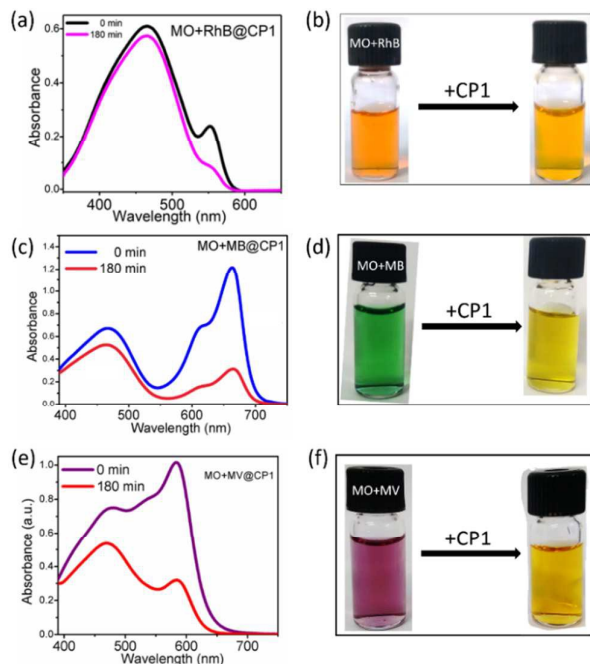


**Fig. 5** (a–f) Selective dye adsorption with mixture of anionic and cationic dyes; UV-Vis spectral changes and digital photographs showing selective adsorption of RhB, MB and MV over MO by **CP1**.

As depicted in Fig. 5, UV-Vis spectra clearly disclosed that absorption intensity of RhB (~553 nm), MB (~662 nm) and MV (~582 nm) decreases significantly, while the MO absorption intensity (~463 nm) showed only marginal decrease. It is also observed by naked eye that color of the mixture of respective dyes in presence of **CP1** after 3 hours of stirring turned to orange, indicating that methyl orange was left in the solution. Both spectroscopic as well as visual detection experiments clearly validate the selective adsorption of respective cationic dyes by **CP1** from the mixture, retaining the MO anionic dye in

the solution. Motivated by the adsorption results of cationic dye, compound **CP1** was employed as a column chromatographic filler for the separation of dyes from water.

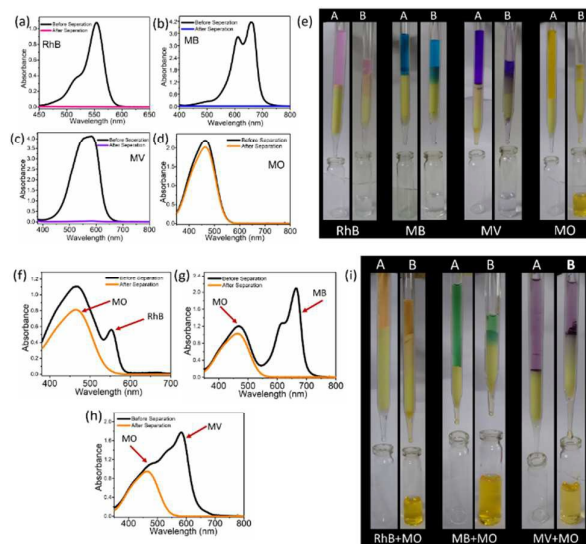
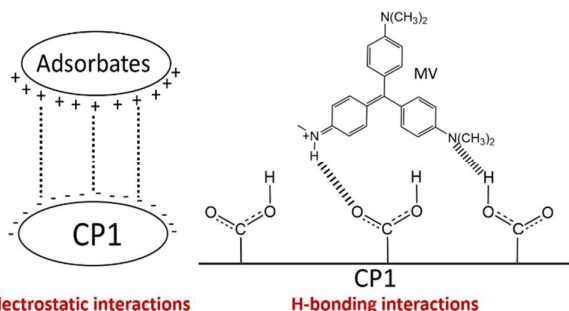


**Fig. 6** (a–d) UV-Vis spectra of aqueous solutions of dye before separation (black) and after separation through the **CP1** chromatographic column (orange) for individual dyes (RhB, MB, MV and MO), (f–h) dye mixture and (e–i) digital photographs illustrating selective separation of cationic dyes by the chromatographic column of **CP1** (A, indicates before separation and B, indicates after separation).

As displayed in Fig. 6, when  $10^{-4}$  M solutions of individual cationic dye stream (RhB, MB and MV) is passed the column and the collected solutions after passing through the column found to be colorless, indicating the separation of dyes from aqueous solutions by adsorption of the column material. Similar experiments were also conducted for mixed-dye combination (RhB+MO, MB+MO and MV+MO) stream passing through the column. The collected solutions after passing through the column displaying pale orange color indicate the presence anionic dye MO in solution and subsequent separation of cationic dyes RhB, MB and MV in the **CP1** column. These results further affirm strongly **CP1** to be an excellent candidate for the efficient and selective adsorption and separation of cationic dyes over anionic dyes.<sup>70-71</sup> There are various factors which can influence the selectivity of specific molecular dye adsorption by MOFs.<sup>72-73</sup> The observed efficient adsorption of **CP1** towards MV from selected pool of cationic dyes may also be explained on the basis of crystal structure analysis. In fact, the concomitant effect of supramolecular/electrostatic interaction between framework and cationic dye molecule as well as accessible layered gap between 2D network to accommodate the dye molecule may probably account for the adsorption of cationic dye by **CP1**. Due to the free/coordinated carboxyl groups which can act as an effective acceptor/donor in H-bonding interactions with the cationic dyes and the layered gap between 2D network structure in **CP1** can induce the adsorption capacity towards cationic dyes by various supramolecular interactions. As revealed in the crystal structure, carboxylate/ carboxylic acid

of the HBTC ligand of **CP1** can act as an active site in supramolecular/electrostatic interaction with the cationic dyes favoring the adsorption process on the surface of the **CP1** host by accommodating the dye molecule between the 2D layers. Probably the uncoordinated carboxylic acid group or the coordinated water oxygen lined on the surfaces of the two-dimensional network can involve in supramolecular interactions via H-bonding with the cationic dye and plays an important role in the adsorption process.



Electrostatic interactions

H-bonding interactions

**Scheme 2** The possible mechanism of dye adsorption on **CP1** by electrostatic and H-bonding interactions.

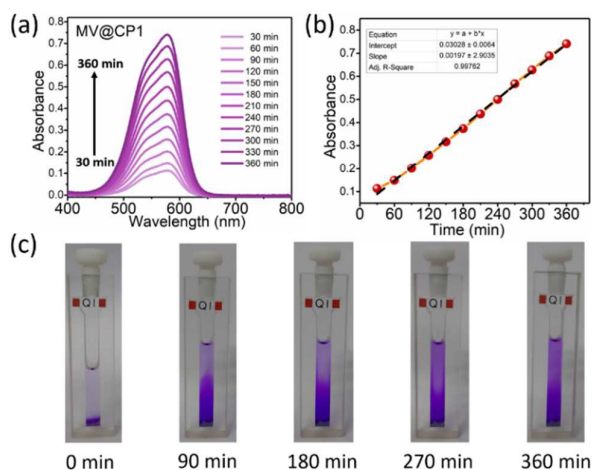


**Fig. 7** (a) Time dependent UV-Vis spectra depicting enhancement in the absorbance ( $\lambda_{\max} = 578 \text{ nm}$ ) suggesting increase in MV release with time, (b) absorbance–time profile showing linear plot for the release of MV (30 to 360 min) and (c) digital photographs showing progressive color change due to release of adsorbed MV in 0.5 mL MeOH after soaking 10 mg of **CP1@MV**.

Hence, the protonated amino nitrogen and free nitrogen atoms of cationic dye MV can comprehend strong N–H...O/O–H...N interactions with the carboxylic group of the BTC moiety of **CP1** in enhancing the adsorption capacity MV up to 97% among other cationic dyes (Scheme 2). Observed decrease in zeta potential ( $\zeta$ ) of **CP1@MV** (–11.5 mV) compared to **CP1** (–21 mV) also corroborate the strong electrostatic interactions between adsorbent and adsorbate (Table S2).<sup>74–75</sup> The desorption process is important and interesting in practical applications. After **CP1** was loaded with the respective cationic dyes, the obtained materials (**CP1@dye**) were soaked in methanol for six hours to accomplish the organic dye release

experiment. Methanol was employed as a releasing media to assess the dye releasing behavior of **CP1@dye**. Fig. 7a–b shows that the adsorbed cationic dye (MV) molecules are progressively released in methanol as represented in UV-Vis spectra indicating the enhancement in the intensity at 578 nm. The same batch study was performed for release of MB and RhB (Fig. S11&S12). The colorless solution gradually changes to the respective dye color (violet) with time indicating the steady release of dye molecule as shown in digital photographs (Fig. 7c).

## Conclusions

In summary, two Zn(II) based mixed ligand luminescent CPs containing N-donor ligand L and rigid aromatic tricarboxylate anions have been synthesized by versatile routes through reactant ratio modulation. Crystal structure revealed that **CP1** is a 2D network composed of  $[\text{Zn}_2(\text{HBTC})_2(\text{H}_2\text{O})_2]_n$  double layered motif linked via terminal nitrogen of L. **CP2** is a 3D framework in which the 2D net,  $[\{\text{Zn}_5(\text{BTC})_2(\text{L})_3(\text{OH})_4(\text{H}_2\text{O})_2\}]_n$  is composed of symmetrically disposed pentanuclear Zn(II) SBUs pillared by L ligands. Both CPs were characterized by various analytical techniques such as CHN, FTIR, TGA and PXRD to evaluate the phase purity and structural integrity. **CP1** was found to exhibit efficient adsorption of cationic dye methyl violet (MV) compared to other cationic dyes including anionic dye methyl orange. In addition, selective adsorption of cationic dye from mixture of dyes, dye release experiments of **CP1** as well as photoluminescence properties of both CPs were also investigated. Selective adsorption of cationic dye by neutral CPs is scantily reported in the literature; simultaneous influence of supramolecular interaction between the carboxylate /water oxygen on the surface of the coordination polymer with the cationic dye and layered gap between 2D network in **CP1** to dwell in the dye moiety may be the probable basis for the adsorption property. Moreover, the chromatographic column of **CP1** shows a preference for separating the cationic dyes and selectivity of cationic dyes from the mixture of cationic and anionic dyes in aqueous solution, highlighting the efficient aqueous–phase separation of organic dyes. Scaling up of **CP1** synthesis and its application is a significant advancement for the methods available as an adsorbent for the aqueous phase separation of cationic dyes and water purification.

## Conflicts of interest

There are no conflicts to declare.

## Acknowledgements

Authors acknowledge the CSIR, India (Project, Grant no. MLP-0017) for financial support, Mr. Parthrajsinh Sodha for TGA data, Ms. Riddhi Laiya for PXRD data, Mr. Viral Vakani for elemental analysis, Ms. Megha Yadav for FTIR data, Mr. Jayesh Chaudhari for FE-SEM images and AESD&CIF for all round

analytical support. YR and BP acknowledge UGC and CSIR (India) for SRF respectively. Authors are grateful to the crystallographic reviewer for providing suggestion and assistance in resolving the problems in the crystal structure analysis. Publication Registration Number: PRIS 105/2017.

## References

- D. R. Baldwin and W. J. Marshall, *Ann. Clin. Biochem.*, 1999, **36**, 267.
- P. J. Harvey, H. K. Handley and M. P. Taylor, *Environ. Sci. Pollut. Res.*, 2015, **22**, 12276.
- M. Farhadian, D. Duchez, C. Vachelard, and C. Larroche, *Water Res.*, 2008, **42**, 1325.
- F. N. V. Hippel, Bulletin of the Atomic Scientists, 2011, **67**, 27.
- S. Farhadi and M. Zaidi, *Appl. Catal. A Gen.*, 2009, **354**, 119.
- K. K. Bisht, Y. Rachuri, B. Parmar and E. Suresh, *J. Solid State Chem.*, 2014, **213**, 43.
- Archana, K. N. Lokesh and R. R. Siva Kiran, *J. Biochem. Tech.*, 2012, **3**, S177.
- C. -P. Li, H. Zhou, S. Wang, H. -H. Yuan, S. -Z. Zhang and M. Du, *Chem. Commun.*, 2017, **53**, 4767.
- F. -I. Hu, Y. -X. Shi, H. -H. Chen and J. -P. Lang, *Dalton Trans.*, 2015, **44**, 18795.
- P. K. Malik, *J. Hazard. Mater.*, 2004, **113**, 81.
- Y. Dong, B. Lu, S. Zang, J. Zhao, X. Wang and Q. Cai, *J. Chem. Technol. Biotechnol.*, 2011, **86**, 616.
- H. Ou, Q. You, J. Li, G. Liao, H. Xia and D. Wang, *RSC Adv.*, 2016, **6**, 98487.
- S. Sansuk, S. Srijaranai and S. Srijaranai, *Environ. Sci. Technol.*, 2016, **50**, 6477.
- I. A. Ibarra, S. Loera, H. Laguna, E. Lima and V. Lara, *Chem. Mater.*, 2005, **17**, 5763.
- H. Laguna, S. Loera, I. A. Ibarra, E. Lima, M. A. Vera, V. Lara, *Microporous Mesoporous Mater.*, 2007, **98**, 234.
- N. A. Khan, Z. Hasan and S. H. Jung, *J. Hazard. Mater.*, 2013, **244**, 444.
- C. Li, Z. Xiong, J. Zhang and C. Wu, *J. Chem. Eng. Data*, 2015, **60**, 3414.
- A. Ayati, M. N. Shahrak, B. Tanhaei and M. Sillanpaa, *Chemosphere*, 2016, **160**, 30.
- P. Lama, H. Aggarwal, C. H. Bezuidenhout and L. J. Barbour, *Angew. Chem. Int. Ed.*, 2016, **55**, 13271.
- I. A. Ibarra, A. Mace, S. Yang, J. Sun, S. Lee, J.-S. Chang, A. Laaksonen, M. Schroder and X. Zou, *Inorg. Chem.*, 2016, **55**, 7219.
- R. G. Miller, P. D. Southon, C. J. Kepert and S. Brooker, *Inorg. Chem.*, 2016, **55**, 6195.
- D. Banerjee, S. K. Elsaidi and P. K. Thallapally, *J. Mater. Chem. A*, 2017, **5**, 16611.
- I. R. Colinas, R. C. Silva and S. R. J. Oliver, *Environ. Sci. Technol.*, 2016, **50**, 1949.
- Q. Zhang, J. Yu, J. Cai, L. Zhang, Y. Cui, Y. Yang, B. Chen and G. Qian, *Chem. Commun.*, 2015, **51**, 14732.
- C. Wang, X. Liu, J. P. Chen and K. Li, *Sci. Rep.*, 2015, **5**:16613.
- M. Mon, F. Lloret, J. Ferrando-Soria, C. Mart.-Gastaldo, D. Armentano and E. Pardo, *Angew. Chem. Int. Ed.*, 2016, **55**, 11167.
- D. Banerjee, W. Xu, Z. Nie, L. E. V. Johnson, C. Coghlan, M. L. Sushko, D. Kim, M. J. Schweiger, A. A. Kruger, C. J. Doonan and P. K. Thallapally, *Inorg. Chem.*, 2016, **55**, 8241.
- L. Zhu, C. Xiao, X. Dai, J. Li, D. Gui, D. Sheng, L. Chen, R. Zhou, Z. Chai, T. E. Albrecht-Schmitt and S. Wang, *Environ. Sci. Technol. Lett.*, 2017, **4**, 316.
- X. Zhu, B. Li, J. Yang, Y. Li, W. Zhao, J. Shi and J. Gu, *ACS Appl. Mater. Interfaces*, 2015, **7**, 223.
- L. Wen, X. Xu, K. Lv, Y. Huang, X. Zheng, L. Zhou, R. Sun, D. Li, *ACS Appl. Mater. Interfaces*, 2015, **7**, 4449.
- X. Zhao, K. Wang, Z. Gao, H. Gao, Z. Xie, X. Du and H. Huang, *Ind. Eng. Chem. Res.*, 2017, **56**, 4496.
- A. C. Kathalikkattil, D. -W. Kim, J. Tharun, H. -G. Soek, R. Roshan and D. -W. Park, *Green Chem.*, 2014, **16**, 1607.
- D. Briones, B. Fernández, A. J. Calahorra, D. Fairen-Jimenez, R. Sanz, F. Martínez, G. Orcajo, E. S. Sebastián, J. M. Seco, C. S. González, J. Llopis and A. Rodríguez-Diéguez, *Cryst. Growth Des.*, 2016, **16**, 537.
- P. Horcajada, R. Gref, T. Baati, P. K. Allan, G. Maurin, P. Couvreur, G. Férey, R. E. Morris and C. Serre, *Chem. Rev.*, 2012, **112**, 1232.
- S. A. A. Razavi, M. Y. Masoomi, T. Islamoglu, A. Morsali, Y. Xu, J. T. Hupp, O. K. Farha, J. Wang and P. C. Junk, *Inorg. Chem.*, 2017, **56**, 2581.
- A. J. Howarth, Y. Liu, P. Li, Z. Li, T. C. Wang, J. T. Hupp and O. K. Farha, *Nat. Rev. Mater.*, 2016, **1**:15018.
- W. Lu, Z. Wei, Z. -Y. Gu, T. -F. Liu, J. Park, J. Tian, M. Zhang, Q. Zhang, T. Gentle III, M. Bosch and H. -C. Zhou, *Chem. Soc. Rev.*, 2014, **43**, 5561.
- Y. Rachuri, B. Parmar, K. K. Bisht, E. Suresh, *Dalton Trans.*, 2017, **46**, 3623.
- J. Heine, M. Hołynska, M. Reuter, B. Haas, S. Chatterjee, M. Koch, K. I. Gries, K. Volz and S. Dehnen, *Cryst. Growth Des.*, 2013, **13**, 1252.
- B. Parmar, Y. Rachuri, K. K. Bisht, R. Laiya and E. Suresh, *Inorg. Chem.*, 2017, **56**, 2627.
- C. Näther, G. Bhosekar and I. Jess, *Inorg. Chem.*, 2007, **46**, 8079.
- D. Banerjee, J. Finkelstein, A. Smirnov, P. M. Forster, L. A. Borkowski, S. J. Teat and J. B. Parise, *Cryst. Growth Des.*, 2011, **11**, 2572.
- A. Karmakar, G. M. D. M. Rúbio, M. F. C. Guedes da Silva, S. Hazra and A. J. L. Pombeiro, *Cryst. Growth Des.*, 2015, **15**, 4185.
- S. Suckert, M. Rams, M. M. Rams and C. Nather, *Inorg. Chem.*, 2017, **56**, 8007.
- R. Seetharaj, P. V. Vandana, P. Arya and S. Mathew, *Arabian J. Chem.*, 2016, DOI:10.1016/j.arabj.2016.01.003.
- B. Parmar, Y. Rachuri, K. K. Bisht and E. Suresh, *ChemistrySelect*, 2016, **1**, 6308.
- Y. Rachuri, B. Parmar, K. K. Bisht and E. Suresh, *Cryst. Growth Des.*, 2017, **17**, 1363.
- K. K. Bisht, P. Patel, Y. Rachuri and E. Suresh, *Acta Crystallogr. Sect. B*, 2014, **B70**, 63.
- G. M. Sheldrick, *SAINT 5.1* ed.; Siemens Industrial Automation Inc., Madison, WI, 1995.
- SADABS, Empirical Absorption Correction Program*; University of Göttingen, Göttingen, Germany, 1997.
- G. M. Sheldrick, *Acta Crystallogr. C*, 2015, **C71**, 3-8.
- A. L. Spek, *Acta Crystallogr. C*, 2015, **71**, 9-18.
- M. Zhang, G. Feng, Z. Song, Y. -P. Zhou, H. -Y. Chao, D. Yuan, T. T. Y. Tan, Z. Guo, Z. Hu, B. Z. Tang, B. Liu and D. Zhao, *J. Am. Chem. Soc.*, 2014, **136**, 7241.
- Z. Hu, W. P. Lustig, J. Zhang, C. Zheng, H. Wang, S. J. Teat, Q. Gong, N. D. Rudd and J. Li, *J. Am. Chem. Soc.*, 2015, **137**, 16209.
- A. Gładysiak, T. N. Nguyen, J. A. R. Navarro, M. J. Rosseinsky and K. C. Stylianou, *Chem. Eur. J.*, 2017, **23**, 13602.
- S. Galli, N. Masciocchi, V. Colombo, A. Maspero, G. Palmisano, F. J. Lopez-Garzon, M. Domingo-Garcia, I. F. andez-Morales, E. Barea and J. A. R. Navarro, *Chem. Mater.* 2010, **22**, 1664.
- A. Ibarra, T. W. Hesterberg, J. -S. Chang, J. W. Yoon, B. J. Holliday and S. M. Humphrey, *Chem. Commun.*, 2013, **49**, 7156.

## ARTICLE

Journal Name

- 58 J. Heine and K. M. Buschbaum, *Chem. Soc. Rev.*, 2013, **42**, 9232.
- 59 W. P. Lustig, S. Mukherjee, N. D. Rudd, A. V. Desai, J. Li and S. K. Ghosh, *Chem. Soc. Rev.*, 2017, **46**, 3242.
- 60 N. Zhao, F. Sun, N. Zhang and G. Zhu, *Cryst. Growth Des.*, 2017, **17**, 2453.
- 61 X. Gao, J. Song, L. X. Sun, Y. H. Xing, F. Y. Bai and Z. Shi, *New J. Chem.*, 2016, **40**, 6077.
- 62 B. -X. Dong, M. Tang, W. -L. Liu, Y. -C. Wu, Y. -M. Pan, F. -Y. Bu and Y. -L. Teng, *Cryst. Growth Des.*, 2016, **16**, 6363.
- 63 Y. Han, S. Sheng, F. Yang, Y. Xie, M. Zhao and J. -R. Li, *J. Mater. Chem. A*, 2015, **3**, 12804.
- 64 Y. Cui, T. Song, J. Yu, Y. Yang, Z. Wang and G. Qian, *Adv. Funct. Mater.*, 2015, **25**, 4796.
- 65 X. -S. Wang, J. Liang, L. Li, Z. -J. Lin, P. P. Bag, S. -Y. Gao, Y. -B. Huang and R. Cao, *Inorg. Chem.*, 2016, **55**, 2641.
- 66 K. Maity and K. Biradha, *Cryst. Growth Des.*, 2016, **16**, 3002.
- 67 C. -Y. Sun, X. -L. Wang, C. Qin, J. -L. Jin, Z. -M. Su, P. Huang and K. -Z. Shao, *Chem. Eur. J.*, 2013, **19**, 3639.
- 68 A. Dey, S. K. Konavarapu, H. S. Sasmal and K. Biradha, *Cryst. Growth Des.*, 2016, **16**, 5976.
- 69 Y. -L. Li, Y. Zhao, Y. -S. Kang, X. -H. Liu and W. -Y. Sun, *Cryst. Growth Des.*, 2016, **16**, 7112.
- 70 S. -R. Zhang, J. Li, D. -Y. Du, J. -S. Qin, S. -L. Li, W. -W. He, Z. -M. Su and Y. -Q. Lan, *J. Mater. Chem. A*, 2015, **3**, 23426.
- 71 S. Han, Y. Wei, C. Valente, I. Lagzi, J. J. Gassensmith, A. Coskun, J. F. Stoddart and B. A. Grzybowski, *J. Am. Chem. Soc.*, 2010, **132**, 16358.
- 72 Y. -X. Hou, J. -S. Sun, D. -P. Zhang, D. -D. Qi and J. -Z. Jiang, *Chem. Eur. J.*, 2016, **22**, 6345.
- 73 Y. -Y. Jia, G. -J. Ren, A. -L. Li, L. -Z. Zhang, R. Feng, Y. -H. Zhang and X. -H. Bu, *Cryst. Growth Des.*, 2016, **16**, 5593.
- 74 P. Horcajada, T. Chalati, C. Serre, B. Gillet, C. Sebrie, T. Baati, J. F. Eubank, D. Heurtaux, P. Clayette, C. Kreuz, J. -S. Chang, Y. K. Hwang, V. Marsaud, P. -N. Bories, L. Cynober, S. Gil, G. Férey, P. Couvreur and R. Gref, *Nat. Mater.*, 2010, **9**, 172.
- 75 F. Leng, W. Wang, X. J. Zhao, X. L. Hu and Y. F. Li, *Colloids Surf., A*, 2014, **441**, 164.